Geophysical Research Letters

RESEARCH LETTER
10.1029/2020GL089509

Volcanically Induced Transient Atmospheres on the Moon: Assessment of Duration, Significance, and Contributions to Polar Volatile Traps

James W. Head[1], Lionel Wilson[1,2], Ariel N. Deutsch[1], Malcolm J. Rutherford[1], and Alberto E. Saal[1]

[1]Department of Earth, Environmental and Planetary Sciences, Brown University, Providence, RI, USA, [2]Lancaster Environment Centre, Lancaster University, Lancaster, UK

Key Points:
- A transient lunar atmosphere from peak volcanic degassing lasting up to ~70 Ma was recently proposed as a source of lunar polar volatiles
- We forward-model individual eruption volume, degassing patterns, and duration of periods between eruptions (repose periods)
- Transient, volcanically induced atmospheres are inefficient sources for volatile delivery to permanently shadowed lunar polar regions

Supporting Information:
- Supporting Information S1

Correspondence to:
J. W. Head,
james_head@brown.edu

Citation:
Head, J. W., Wilson, L., Deutsch, A. N., Rutherford, M. J., & Saal, A. E. (2020). Volcanically induced transient atmospheres on the moon: Assessment of duration, significance, and contributions to polar volatile traps. *Geophysical Research Letters*, *47*, e2020GL089509. https://doi.org/10.1029/2020GL089509

Received 7 JUN 2020
Accepted 1 SEP 2020
Accepted article online 9 SEP 2020

Abstract A transient lunar atmosphere formed during a peak period of volcanic outgassing and lasting up to about ~70 Ma was recently proposed. We utilize forward-modeling of individual lunar basaltic eruptions and the observed geologic record to predict eruption frequency, magma volumes, and rates of volcanic volatile release. Typical lunar mare basalt eruptions have volumes of ~10^2–10^3 km^3, last less than a year, and have a rapidly decreasing volatile release rate. The total volume of lunar mare basalts erupted is small, and the repose period between individual eruptions is predicted to range from 20,000 to 60,000 years. Only under very exceptional circumstances could sufficient volatiles be released in a single eruption to create a transient atmosphere with a pressure as large as ~0.5 Pa. The frequency of eruptions was likely too low to sustain any such atmosphere for more than a few thousand years. Transient, volcanically induced atmospheres were probably inefficient sources for volatile delivery to permanently shadowed lunar polar regions.

Plain Language Summary Could gas emitted from volcanic eruptions during the most intense and voluminous period of lunar mare volcanism produce a temporary lunar atmosphere? Could the presence of such an atmosphere enable volatiles to reach the cold traps in the permanently shadowed regions at the lunar poles? We use information from lunar geology and sample analyses to predict the number of eruptions with time, the volume of individual eruptions, the rates of volcanic gas release during each eruption, and the time between eruptions. We find that only under rare circumstances could a single eruption or two eruptions closely spaced in time release enough gas to create a transient atmosphere with a pressure as large as ~0.5 Pa. Furthermore, it is difficult to sustain such an atmosphere for more than a few thousand years. These results suggest that volcanically produced atmospheres are inefficient source mechanisms for delivery of volatiles to form deposits in permanently shadowed polar regions of the Moon; this favors volatile-rich impactors as the major source of polar ice.

1. Introduction

The current atmosphere of the Moon is a stable, low-density surface boundary exosphere (~10^{-12} mbar) (Benna et al., 2015; Cook et al., 2013; Stern, 1999) and is thought to have changed little in the last several billion years. Volcanism, a significant source of volatile supply to planetary atmospheres throughout planetary history, is known to have been much more important in early lunar history (mare basalt volcanism; Shearer et al., 2006; Head & Wilson, 2017), spanning from over 4 billion years ago (beginning with cryptomaria; Whitten & Head, 2015a, 2015b), reaching peak fluxes between 3 and 4 Ga, and declining to much lower levels between 3 and 1 Ga (Head & Wilson, 2017; Hiesinger et al., 2011; Pasckert et al., 2015).

Needham and Kring (2017) assessed lunar mare basalt volcanic flux estimates and volatile release abundances to address whether these patterns might lead to a transient or sustained lunar atmosphere early in lunar history. Using the distribution and quantity of mare basalt fill, and estimates of its age, they calculated the magma flux (the volume of mare basalt erupted as a function of time), and then estimated the corresponding release rate of volatiles on the basis of estimates derived from the analysis of lunar samples (e.g., Hauri et al., 2011; Kring, 2014; Rutherford & Papale, 2009; Saal et al., 2008). Using estimates of mare basalt unit ages (e.g., Hiesinger et al., 2011) and thicknesses (Weider et al., 2010), Needham and Kring (2017) concluded that during a period of peak mare emplacement and volcanic volatile release at ~3.5 Ga (supporting

information Figures S1a and S1b), the maximum atmospheric pressure at the lunar surface could have reached ~1 kPa (~1.5 times greater than the current atmospheric surface pressure of Mars) (Figure S1c) and that this lunar atmosphere could have persisted for ~70 million years before fully dissipating (Figure S1c). They further pointed out that even though most of the volcanically released volatiles will have been lost to space, if only 0.1% of the water released during these eruptions migrated to the permanently shadowed polar regions of the Moon, then the resulting hydrogen mass could account for the entire currently observed hydrogen deposits located there (Eke et al., 2009; Livengood et al., 2018).

We adopt a different approach, using improved models of the generation, ascent, and eruption of lunar basaltic magma (Wilson & Head, 2017), to predict flow volumes, eruption frequencies (Head & Wilson, 2017), and temporal magmatic volatile release patterns in individual eruptions (Rutherford et al., 2017; Wilson & Head, 2018). Key components of this analysis are (1) the range (and mean value) of magma volumes erupted in individual eruptions, (2) the masses, and hence volumes, of the various gases released in any one eruption, (3) the duration of the eruption and the gas release rate (varying significantly as the eruption progresses), (4) the typical time intervals between eruptions (repose periods) as a function of geologic time, and (5) the timescale for the dissipation of an atmosphere once one is emplaced. We review the geological basis for the first four components, examine the potential time-dependence and variability of gas release in an individual typical eruption, and finally address the question: Are these gas-release values sufficient to form a transient atmosphere and, if so, for what duration? We then compare our findings with the broad-scale, time-averaged peak flux estimates of Needham and Kring (2017) (see the supporting information), and address similarities and differences and their causes, and how estimates might be refined in the future. We conclude by assessing whether the forward-modeling predictions of gas-release rates are sufficient to (1) act as a significant supply of volatiles to the permanently shadowed lunar polar cold-trap regions and (2) form a transient lunar atmosphere for a period sufficient to favor astrobiological activity as suggested by Schulze-Makuch and Crawford (2018).

2. Forward Modeling Lunar Mare Basaltic Eruptions

Wilson and Head (2017) and Head and Wilson (2017) improved earlier theoretical models for the generation, ascent, and eruption of basaltic magma on the Moon (Head & Wilson, 1992; Wilson & Head, 1981) by using new data on crustal thickness and density (Wieczorek et al., 2013), magma volatile inventories (Rutherford et al., 2017), and surface morphology, topography, and structure (from Lunar Reconnaissance Orbiter). They showed that ongoing partial melting in buoyant diapirs deep in the mantle overpressurizes the source regions, producing sufficient stress to cause brittle fracturing; a magma-filled crack grows, disconnects from its source and propagates to the surface as a blade-shaped, convex-upward dike. The typical turbulent magma rise speeds that result are ~10 to a few tens of m s^{-1}, dike widths are ~100 m, and eruption rates from 1–10 km long fissure vents are ~10^5 to 10^6 m^3 s^{-1}. Lunar eruption volume fluxes derived from lava sinuous rille lengths and depths or flow thicknesses and surface slopes are ~10^5 to 10^6 m^3 s^{-1} (volume-limited lava flows) and >10^4 to 10^5 m^3 s^{-1} (rilles). The volume of magma released in one event is predicted to be in the range 10^2–10^3 km^3 (Head & Wilson, 2017; Wilson & Head, 2017). Thus, if all the magma were extruded from these dike events and spread evenly across the surface in 25 m thick flows, they would occupy areas of 4,000 to 40,000 km^2, well within the range of thicknesses and areas of mapped and dated (e.g., Hiesinger et al., 2011) lunar mare lava flows. We now summarize aspects of these treatments to derive the relevant parameters.

2.1. Individual Mare Basalt Eruption Volumes: Range and Typical Values

Individual eruption volumes of typical visible, and therefore most recent, lava flow deposits, are at least ~200–300 km^3 (Head & Wilson, 2017) (Table 1). In addition, Head and Wilson (1981) estimated the minimum volume of lava, ~100 km^3, needed to thermo-mechanically erode the preserved sinuous rille channels. Applying the same method to the largest lunar rille, Schroeter's Valley, implies a volume of 2,000 km^3 and a duration of ~150 days. On the basis of these predictions and observations, we adopt a range of individual eruption volumes, V, of 100–2,000 km^3 (Table 1), with typical values in the range 100–300 km^3.

2.2. Total Mare Basalt Erupted Volumes

Using mare basin lava fill depth estimates, the total volume, V_t, of all volcanic products erupted on the Moon over its lifetime is ~10^7 km^3 (Evans et al., 2016; Head & Wilson, 1992). The absolute dates of specific

Table 1
Parameters of Various Types of Lunar Eruption

Feature	V/km^3	F_l/(m^3 s^{-1})	τ_e/days	M_g/kg	F_g/(kg s^{-1})
Cobra Head	2,000	1.4×10^5	150	1.2×10^{13}	9.3×10^5
Long flow	300	~10^5	30	1.8×10^{12}	6.9×10^5
Small flow	200	~10^4	100	1.2×10^{12}	1.4×10^5
Sinuous rille	100	~3×10^4	50	~6×10^{11}	1.4×10^5

Note. Cobra Head is the source vent of Schroeter's Valley (Head & Wilson, 2017). Released volatiles assumed to have molecular mass 31.4 kg kmol^{-1} and to form n = 2,000 ppm by mass of a magma that has a liquid density ρ_m = 3,000 kg m^{-3}. V = lava volume; F_l = lava volume eruption rate; τ_e = eruption duration; M_g = total gas mass released; F_g = gas mass release rate. Typical values for parameters are quoted, but individual eruption values may vary by a factor of at least 2 to 3.

eruptions are unknown, but crater size-frequency distribution-derived dates of units mapped from orbit, and stratigraphic relationships, imply that the overall time span of the vast majority of lunar volcanic activity was ~2 Ga (Head & Wilson, 2017; Head & Wilson, 2017; Hiesinger et al., 2011).

2.3. Number of Eruptions, Average Eruption Rates, and Estimated Repose Periods

Using the 100–300 km^3 average eruption volume, the ~10^7 km^3 total erupted volume of mare basalts, and the ~2 Ga duration of volcanism, we calculate a total of ~30,000 to 100,000 eruptions with an average repose period of 20,000 to 60,000 years. These repose times assume that eruptions occur randomly in space and time, in which case two eruptions might occur with a much smaller time interval; however, we show in the supporting information that eruptions at intervals close enough in time to influence our conclusions will be rare. Accounting for lunar thermal evolution (conductive cooling and lithospheric thickening) in terms of mare mantle production rates and the evolving lithospheric stress state and magnitude (Head & Wilson, 2017), we would predict decreasing volumes of magma with time. If three times as much magma was erupted in the 4–3 Ga period than in the 3–2 Ga period, for example, the earlier eruptions would have occurred every 13,000 to 40,000 years.

2.4. Eruption Durations

Analyses of the dynamics of lunar eruptions allow us to estimate the volume fluxes, F_l, of lava forming surface flows and sinuous rilles (Head & Wilson, 2017; Wilson & Head, 2017); coupled with the typical erupted volumes described above, these give values for the typical durations, τ_e, of these eruptions (Table 1), all less than 6 months, with most eruption durations in the 1–3 month range.

2.5. Magmatic Volatiles and Volatile Release Patterns

Analyses of lavas and pyroclastics sampled by the Apollo missions (Chen et al., 2015; Hauri et al., 2011; Ni et al., 2019; Renggli et al., 2017; Rutherford et al., 2017; Rutherford & Papale, 2009; Saal et al., 2008) provide estimates for the compositions and amounts of released volatiles. The highest amount is that for picritic magmas, ~3,400 ppm (Rutherford et al., 2017). At the other extreme, Head and Wilson (2017) found that the radii of the lava ponds feeding the lava flows eroding sinuous rille channels imply total magma volatile contents of no more than 700 ppm. We adopt 2000 ppm, close to the average of these extremes. The Rutherford et al. (2017) volatiles are CO, H_2O, SO_2, H_2S, COS, and F present in amounts n_i of 1,395, 1,133, 327, 168, 327, and 50 ppm, respectively, and with molecular masses m_i of 28.0, 18.0, 64.1, 34.1, 60.1, and 19.0, respectively, the mean molecular weight is $\Sigma (n_i m_i)/\Sigma n_i$ = 31.4 kg kmol^{-1}. The corresponding values for alternative compositions suggested by Renggli et al. (2017) and Newcombe et al. (2017) are 48.9 and 22.2 kg kmol^{-1}, respectively; we adopt the Rutherford et al. (2017) value as typical for subsequent calculations.

2.6. Volatile Input to the Atmosphere

We first calculate the *total volume of gas released* from an eruption of a specific volume and then analyze the *time-history of gas release in the several phases of an individual eruption* (Rutherford et al., 2017; Wilson & Head, 2018). Multiplying the dense-rock-equivalent erupted volume V by the typical density of lunar basaltic magma, ρ_m = ~3,000 kg m^{-3}, yields the magma mass erupted, and multiplying that by the total released gas mass fraction $n_t = \Sigma n_i$ gives the total gas mass released, M_g. Finally dividing M_g by τ_e yields the average gas

mass input rate to the atmosphere, F_g. Table 1 summarizes these values. However, gas release during an eruption is nonlinear and typically declines with time (Wallace et al., 2015). Speciation, relative abundances and fluxes of specific volatiles can vary during a single eruption. Could such variations in individual volcanic eruptions result in spikes in volatile output contributing to an atmosphere that might be underestimated by deriving an average value for the entire eruption? We now employ an updated version of a recent model of the typical phases of a lunar eruption to assess these questions.

Wilson and Head (2018), using data from Rutherford et al. (2017), assessed mare basalt gas release patterns during individual volcanic eruptions as a basis for predicting the effect of sequential gas production, bubble nucleation and growth, magma and gas rise rates, bubble coalescence, and magma disruption processes. Subdividing typical lunar eruptions into four phases (Figure 1a), they showed how these phases of mare basalt eruption, together with total dike volumes, initial magma volatile content, vent configuration, and magma discharge rate, could assist in relating the wide range of seemingly disparate volcanic features to a common set of eruption processes. Figure 1 updates the values given by Wilson and Head (2018) using a more detailed integration of the eruption rate model based on work in progress.

In Phase 1, which is very short-lived, the rising dike penetrates to the surface and initiates *the transient gas release phase*. This very explosive phase is due to concentration of volatiles into a low-pressure area near the upper propagating dike tip (Wilson & Head, 2003). Pure gas may extend 100–200 m down from the top of the dike, above a high vesicularity foam layer extending downward ~10 km. Eruption of this gas-rich magma dike tip takes as little as a few minutes, resulting in an extremely thin but very widespread deposit, consistent with volcanic glass beads ubiquitous in lunar soils.

During Phase 2, *the high-flux hawaiian eruptive phase*, the dike continues to rise toward a neutral buoyancy configuration. This phase is characterized by the highest magma discharge rate during the eruption, ~10^6 m^3/s, involving a near-steady explosive magma eruption; the volatile content is representative of the bulk of the magma. This phase is characterized by formation of a relatively steady hawaiian fire fountain, largely optically dense. Submillimeter-sized pyroclastic droplets lose gas efficiently and accumulate with negligible cooling within a few to 10 km of the fissure, forming a lava lake deficient in gas bubbles. For a short-lived eruption, lava that is largely degassed flows away from the lake, initially turbulently, to form the distal part of the final lava flow deposit. For a sufficiently long-lasting eruption, the lava will feed a flow eroding a sinuous rille. More than 80% of the total dike magma volume would have been erupted during this phase; the erupted magma volume flux decreases from ~10^6 to ~10^5 m^3 s^{-1} over its typical 2–3 day duration.

Phase 3, the lower flux *hawaiian to strombolian transition phase* begins when the positive buoyancy of the lower part of the dike in the mantle balances the negative buoyancy of the upper part in the crust and the eruption-feeding dike approaches an equilibrium. The lower dike tip stops rising, and fixing the vertical extent of the dike. The main driving process in this phase becomes the horizontal reduction in dike thickness due to (1) decrease in internal excess pressure and (2) relaxation of forced host rock deformation due to initial dike intrusion (Wilson & Head, 2017). Shallow crust host rock deformation is probably elastic and rapid; hotter mantle rock deformation (surrounding the lower part of the dike) is more likely to be visco-elastic or viscous; this results in a much longer closure timescale. Magma vertical rise speed in the dike decreases greatly (to less than 1 m s^{-1}) during this period; this implies that the magma volume flux leaving the vent decreases similarly to a few $\times 10^4$ m^3 s^{-1} during ~3–5 days. Reduction in vertical magma flow speed means that nucleating gas bubbles throughout the dike vertical extent can now rise through the liquid at an appreciable rate. There is ample time for larger bubbles to overtake smaller bubbles (especially CO bubbles being produced at great depths). This leads to coalescence and even greater growth; this in turn leads to very large bubbles—gas slugs—filling almost all of the dike width and producing strombolian surface explosions (Parfitt & Wilson, 1995). The transition from hawaiian activity (Phase 2) to strombolian (Phase 3) occurs rapidly.

Phase 4, the *dike closing*, *strombolian vesicular flow phase*, begins when the activity becomes entirely strombolian. Horizontal dike closure continues due to tectonic stresses, and magma is extruded at a low flux. Magma from the deepest dike parts continues to be forced upward to lower pressure levels thus continuing to produce some CO at all depths; the result is very minor but continuing strombolian explosive activity above the vent. For magma still emerging from the vent, a stable crust will form and flow away as lava.

Two different pathways might occur during Phase 4 activity. In *low flux eruptions* (Phase 4a), Phase 4 might begin following the eruption of most of the magma in the dike, and the volume flux has decreased to a very

Eruption Phase	PHASE 1	PHASE 2	PHASE 3	PHASE 4
	Dike penetrates to surface, transient gas release phase	Dike base still rising, high flux hawaiian eruptive phase	Dike equilibration, lower flux hawaiian to strombolian transition phase	Dike closing, strombolian vesicular flow phase
Dike Configuration	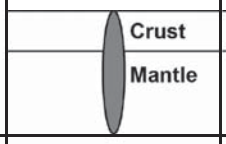	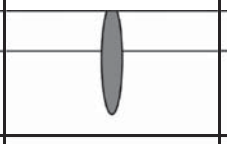	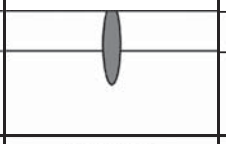	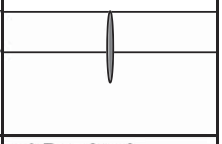
Surface Eruption Style	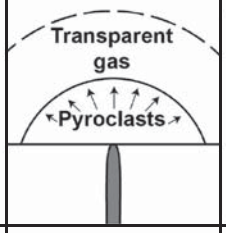	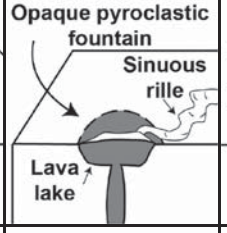	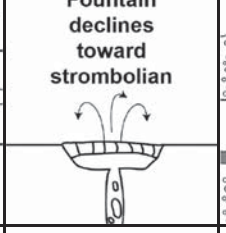	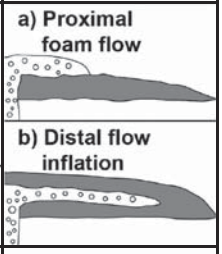
Magma Rise Speed	30 to 20 m/s	20 to 10 m/s	5 to <1 m/s	< 1 m/s
Magma Volume Flux	~10^6 m^3/s	10^6 to 10^5 m^3/s	10^5 to ~10^4 m^3/s	~10^4 m^3/s
Percent Dike Volume Erupted	<5%	~80%	~5%	~10%
Phase Duration	~3 minutes	~4 day	~6 day	~30 days

(a)

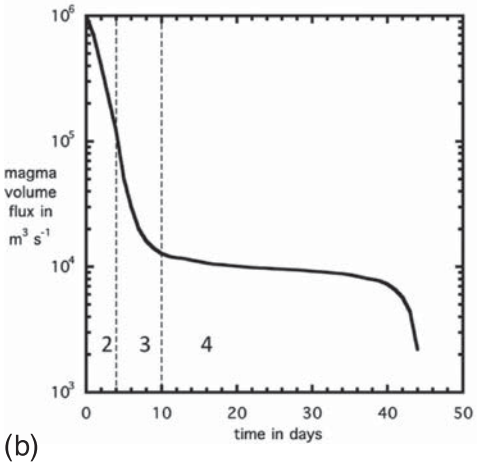

(b)

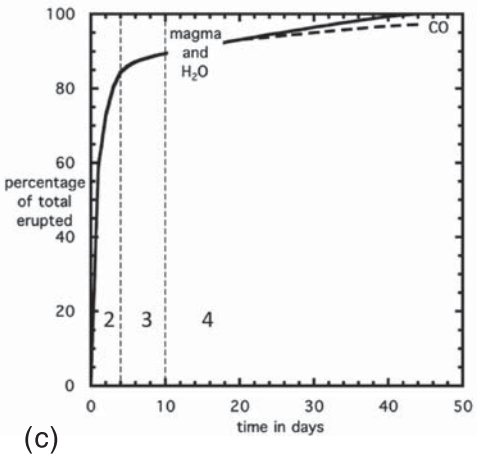

(c)

Figure 1. Forward modeling results for a 250-km^3 lunar volcanic eruption. (a) The characteristics of four eruptive phases during the eruption with diagrams and parameters representing typical values. The relative duration of individual phases depends on total dike volume and vertical extent. (b) Magma volume flux for the typical eruption in (a) as a function of time. (c) Percentage of total magma and gas released as a function of time. Vertical broken lines in parts (b) and (c) separate labeled phases; Phase 1 is too brief to be visible.

low level (Figure 1a). Wilson and Head (2017) predicted that the result will be the emplacement of vesicular lava in the vicinity of the vent as a series of cooling-limited flows potentially building a small, low shield. Erupted magma consists of liquid which contains bubbles (a mixture of gases and volatile elements) (Gaillard & Scaillet, 2014; Renggli et al., 2017; Saal et al., 2018). These are determined by the thermodynamic equilibrium between the products of interactions (mainly between H_2O and sulfur species) released over the last <500 m of magma flux. Such gas bubbles would nucleate with diameters of ~10–20 μm and grow to ~20–30 μm at the surface; they remain stable within the lava (surface tension forces impose a retaining pressure of ~30 kPa; Wilson & Head, 2017). Lavas exsolving ~1,000 ppm of such gases would leave the vent as lava foams with vesicularities >90% by volume. The topmost bubbles would likely have exploded into the overlying vacuum; this should produce a layer of bubble wall shards, and gas escapes easily through this accumulating debris layer until welding of particles and accumulated debris weight inhibited further foam disintegration. If the underlying lava still contained dissolved volatiles, the unvesiculated layer could become important during further lava cooling and crystallization if volatile concentration into the remaining liquid resulted in second boiling and additional postemplacement vesiculation. Volatile contributions to the atmosphere of these latter-stage processes would be minimal, however, as the rates of diffusive volatile loss from vesiculated cooling and cooled lavas are extremely low.

A second potential outcome is predicted to occur in dikes that are vertically more extensive (Phase 4b, high flux). If a large fraction of total dike magma remains available for extrusion as vesicular lava, this lava can readily intrude into the still-hot interiors of the previously emplaced nonvesicular flows and cause flow inflation. The shallow parts (<400 m depth) of a dike feeding such intruding/inflating flows would contain not yet exsolved water and sulfur compounds. The resulting inflated flows would cool on a timescale of weeks: Volatile concentration into the residual liquid as crystallization occurred would then lead to second boiling. The new population of gas bubbles could cause a possibly extensive further inflation episode (Wilson et al., 2019). The resulting magmatic foam and gas could escape through cracks in the lava crust caused by inflation, but again the gas flux into the atmosphere would be minimal.

Eruption Phase 4 duration is controlled by the global stress state of the lithosphere (both its nature and magnitude), influencing host rocks visco-elastic relaxation, and by magma cooling in the dike. Lunar thermal history (Solomon & Head, 1980) suggests extensional lithospheric stresses during the first ~1 Ga, followed by compressive stresses at ~3.6 Ga as the interior cooled. This would encourage more closure of dikes in geologically more recent eruptions. Dike models (Wilson & Head, 2017) predict that Phase 4 dikes had initial widths of at least 10–20 m. Cooling and solidification by conduction alone of near-stagnant magma in such dikes would occur 1–2 years after the end of an eruption.

In summary, the majority of the volume of magma erupted during a typical lunar eruption occurs in Phases 2 and 3 (Figure 1a). The rise speed of magma during these phases is so large that gas bubbles stay locked to the magma, and so the vast majority of gas release into the atmosphere during a lunar eruption also occurs during Phases 2 and 3, phases that take place over about 5–10 days, less than about 25% of the total eruption duration. We now turn to a discussion of the implications of the (1) total gas release patterns and (2) gas release patterns in individual eruptions, for the formation of a transient lunar atmosphere.

3. Discussion

The relevant parameters (lava volume, eruption rate, duration, total gas released, gas mass release rate, etc.) for several types and scales of lunar eruptions (short flow, long flow, sinuous rille, and Cobra Head/Schroeter's Valley, the largest known lunar eruption) are shown in Table 1. For each of the released gas masses we find the properties of the lunar atmosphere that would be created if the gas release rate from the erupted magma was much greater than the total loss rate of the atmosphere into space by whatever mechanisms were relevant (which we shall show shortly is the case). Using the mean molecular mass m = ~31.4 kg/kmol described above, we find the scale height of the resulting atmosphere, $H = (Q\ T)/(m\ g)$ where Q is the universal gas constant, 8.314 kJ kmol^{-1} K^{-1}, T is the mean lunar surface temperature, ~270 K assuming radiative equilibrium and a 25% dimmer Sun ~3.5 Ga ago, and g is the acceleration due to gravity at the lunar surface, 1.62 m s^{-2}. These values give H = 44.1 km. The surface density of the atmosphere, ρ_s, is equal to its mass, M, from Table 1, divided by the volume equivalent to the surface area of the Moon multiplied by the scale height, that is, $\rho_s = M/(4\ \pi\ R^2\ H)$ where R is the lunar radius, 1,738 km.

Table 2
Initial Values of the Surface Density, ρ_s, and Surface Pressure, P_s, in a Transient Atmosphere Produced by the Four Types of Volcanic Activity Listed in Table 1

Feature	ρ_s/(kg m^{-3})	P_s/Pa	τ_d/years
Cobra Head	7.2×10^{-6}	0.51	38,000
Long flow	1.1×10^{-6}	7.7×10^{-2}	5,700
Small flow	7.2×10^{-7}	5.1×10^{-2}	3,800
Sinuous rille	3.6×10^{-7}	2.6×10^{-2}	1,900

Note. The maximum duration of the atmosphere, τ_d, is indicated.

Finally, the surface pressure is $P_s = \rho_s g H$. Table 2 lists the values of ρ_s and P_s corresponding to the eruption types in Table 1. Assuming the most extreme alternative volatile species mixture suggested in the literature, the sulfur-dominated mixture of Renggli et al. (2017) would increase m by a factor close to 1.5. This would decrease the scale height and increase the surface density of the atmosphere by the same factor and leave the surface pressure unchanged.

The implied atmospheric gas masses due to the typical types of lunar volcanic activity in Table 1 are of order 10^{12} to 10^{13} kg. As part of an extensive review of three possible types of lunar atmosphere, Stern (1999; his section 5.2.2) treated a hypothetical volcanically induced atmosphere with a total gas mass of 10^{11} kg and adopted the loss rate calculated by Vondrak (1974) of 10 kg s^{-1}. The same loss rate is estimated in a recent more general analysis by Aleinov et al. (2019) treating much more massive, at least ~10^{15} kg, atmospheres with surface pressures >100 Pa. Using a 10 kg s^{-1} loss rate leads to the typical timescales for atmospheric decay, τ_d, shown in Table 2, between ~2,000 and ~6,000 years. These values need to be compared with the likely intervals between eruptions on the Moon. As shown earlier, with a total volume of volcanics of V_t = ~10^7 km^3 (Evans et al., 2016; Head & Wilson, 1992), a typical erupted volume of 200 ± 100 km^3 (Table 1), and a total duration of volcanism of τ_d = ~2 Ga, the shortest average interval between eruptions is ~13,000 to 40,000 years in the early part of the mare volcanism era if eruptive activity decreases with time. Increasing the 2,000 ppm magmatic volatile mass fraction used here to the 3,400 ppm suggested by Rutherford et al. (2017) would increase the atmospheric mass values in Table 1 by a factor of 1.7, but this would still make the timescale for atmosphere loss a factor of ~4 less than the average time between eruptions.

What effect does the nonlinear release of gas during the four phases of a typical volcanic eruption (Figure 1a) have on the peak loss of volatiles during an eruption? To address this question, we first look at the magma volume eruption rate as a function of time for an eruption releasing 250 km^3 of magma (a medium-scale volume in the ~100–300 km^3 average eruption volume range described above) and lasting 46 days (about average for the 1–3 month range discussed above) (Figure 1b). Magma volume flux is clearly highest in the first 10 days (Phases 1 and 2), decreasing two orders of magnitude from an initial peak flux of 10^6 m^3 s^{-1}, to 10^4 m^3 s^{-1} after ~10 days. Magma volume flux remains at this low value for the next 30 days (Phases 3–4) before falling to zero in the last 4 days at the end of the eruption. Thus, ~90% of the total volume of magma erupted is emplaced in Phase 2, the hawaiian phase characterized by maximum magma degassing and volatile loss.

Using the magma volatile species proposed by Rutherford et al. (2017), the percentages of the magma, water, and CO released as a function of time in the same eruption are shown in Figure 1c. Released water closely mimics the erupted magma, unless a significant amount is left trapped in late-stage magma (Phase 4) intruded into earlier flow lobes during flow inflation. If significant inflation occurs, and the inflating gas does not escape, about 95% of the water would be released instead of 100% as shown in Figure 1c. The CO in the magma, preferentially released at very great depth, does not all escape: CO released in Phase 4 does not have time to reach the surface before the conduit freezes, even allowing for bubble coalescence and rise. However, this only represents a few percent of the total CO and so almost all of the total is released.

In summary, the implied intervals between typical lunar eruptions, ~13,000 to 40,000 years, are 6–7 times greater than the likely durations of the vast majority of individual transient atmospheres, between ~2,000 and 6,000 years. Only for the single, extreme example of Cobra Head/Schroeter's Valley are the time scales comparable. Otherwise, only if all of the Moon's ~ 10^7 km^3 of basaltic volcanism were to have taken place within a 300 Ma interval would the time scales generally be comparable. The nonlinear release of gas during the four phases of a single eruption do not alter this conclusion; even though volatile release is concentrated in the first 25–35% of the eruption, the long repose periods between eruptions preclude sufficient buildup to create an enduring atmosphere. The same is true of leakage of gas from magma reservoirs between eruptions: If half of a typical magma volatile inventory is released uniformly over the ~40 ka average interval between eruptions, the leakage rate is somewhat less than 1 kg s^{-1}, an order of magnitude less than the atmospheric loss rate.

4. Conclusions

On the basis of our analysis of the generation, ascent, and eruption of lunar mare basalt magmas and forward-modeling individual eruptions, we conclude that it is very unlikely that the Moon had a semipermanent (as long as ~70 Ma) volcanically driven atmosphere as proposed by Needham and Kring (2017), even during a period of peak volcanic flux in early lunar history. We attribute the differences between our estimates and those of Needham and Kring (2017) (see discussion in supporting information) to their use of maximum impact basin depths as average depths and assignment of all excess volumes below datable units to one age (e.g., 5.9×10^6 km^3 assigned to 3.5 Ga in the case of Imbrium).

We also conclude that these low volatile release volumes and rates are not conducive to optimizing the transport of released volatiles from the eruption site to the poles to enhance the accumulation of volatiles in polar cold traps (see also Aleinov et al., 2019), nor of creating temporary environments that might favor astrobiological activity (Schulze-Makuch & Crawford, 2018). Our results suggest that most volatiles in lunar polar cold traps originated from volatile-rich impacts, rather than volatile release from volcanic eruptions, similar to findings about polar cold-trap volatile deposits on Mercury (e.g., Deutsch et al., 2019, 2020; Ernst et al., 2018). This issue could be clarified for the Moon by in situ D/H ratio measurements. In order to refine our volcanic emission estimates, future lunar exploration goals should include further analysis of detailed lava flow thicknesses, ages, volumes, volatile contents, and repose periods, as well as better determination of the interior structure of mare deposits in large impact basins.

Acknowledgments

We gratefully acknowledge financial support from: the NASA Lunar Reconnaissance Orbiter (LRO) Mission, Lunar Orbiter Laser Altimeter (LOLA) Experiment Team (Grants NNX11AK29G and NNX13AO77G) (J. W. H.); the Leverhulme Trust for funding through an Emeritus Fellowship (L. W.); the NASA Harriett G. Jenkins Graduate Fellowship (Grant 80NSSC19K1289) (A. N. D.). No new data were produced or archived in this analysis.

References

Aleinov, I., Way, M. J., Harman, C., Tsigaridis, K., Wolf, E. T., & Gronoff, G. (2019). Modeling a transient secondary paleolunar atmosphere: 3-D simulations and analysis. *Geophysical Research Letters*, *46*, 5107–5116. https://doi.org/10.1029/2019gl082494

Benna, M., Mahaffy, P. R., Halekas, J. S., Elphic, R. C., & Delory, G. T. (2015). Variability of helium, neon, and argon in the lunar exosphere as observed by the LADEE NMS instrument. *Geophysical Research Letters*, *42*, 3723–3729. https://doi.org/10.1002/2015gl064120

Chen, Y., Zhang, Y., Liu, Y., Guan, Y., Eiler, J., & Stolper, E. (2015). Water, fluorine, and sulfur concentrations in the lunar mantle. *Earth and Planetary Science Letters*, *427*, 37–46. https://doi.org/10.1016/j.epsl.2015.06.046

Cook, J. C., Stern, S. A., Feldman, P. D., Gladstone, G. R., Retherford, K. D., & Tsang, C. C. C. (2013). New upper limits on numerous atmospheric species in the native lunar atmosphere. *Icarus*, *225*(1), 681–687. https://doi.org/10.1016/j.icarus.2013.04.010

Deutsch, A. N., Head, J. W. III, & Neumann, G. A. (2019). Age constraints of Mercury's polar deposits suggest recent delivery of ice. *Earth and Planetary Science Letters*, *520*, 26–33. https://doi.org/10.1016/j.epsl.2019.05.027

Deutsch, A. N., Head III, J. W., Parman, S. W., Wilson, L., Neumann, G. A., & Lowden, F. (2020). *The mass flux of volatiles from effusive eruptions on mercury* (LPI Contribution No. 2326, p. 2259). The Woodlands, TX: Paper presented at Lunar and Planetary Science Conference.

Eke, V. R., Teodoro, L. F. A., & Elphic, R. C. (2009). The spatial distribution of polar hydrogen deposits on the moon. *Icarus*, *200*(1), 12–18. https://doi.org/10.1016/j.icarus.2008.10.013

Ernst, C. M., Chabot, N. L., & Barnouin, O. S. (2018). Examining the potential contribution of the Hokusai impact to water ice on mercury. *Journal of Geophysical Research: Planets*, *123*, 2628–2646. https://doi.org/10.1029/2018JE005552

Evans, A. J., Soderblom, J. M., Andrews-Hanna, J. C., Solomon, S. C., & Zuber, M. T. (2016). Identification of buried lunar impact craters from GRAIL data and implications for the nearside Maria. *Geophysical Research Letters*, *43*, 2445–2455. https://doi.org/10.1002/2015GL067394

Gaillard, F., & Scaillet, B. (2014). A theoretical framework for volcanic degassing chemistry in a comparative planetology perspective and implications for planetary atmospheres. *Earth and Planetary Science Letters*, *403*, 307–316. https://doi.org/10.1016/j.epsl.2014.07.009

Hauri, E. H., Weinreich, T., Saal, A. E., Rutherford, M. C., & Van Orman, J. A. (2011). High pre-eruptive water contents preserved in lunar melt inclusions. *Science*, *333*(6039), 213–215. https://doi.org/10.1126/science.1204626

Head, J. W., & Wilson, L. (1981). *Lunar sinious rille formation by thermal erosion: Eruption conditions, rates and durations* (Vol. XII, pp. 427–429). Paper presented at Lunar and Planetary Science Conference.

Head, J. W., & Wilson, L. (1992). Lunar mare volcanism: Stratigraphy, eruption conditions, and the evolution of secondary crusts. *Geochimica et Cosmochimica Acta*, *56*(6), 2155–2175. https://doi.org/10.1016/0016-7037(92)90183-J

Head, J. W. III, & Wilson, L. (2017). Generation, ascent and eruption of magma on the moon: New insights into source depths, magma supply, intrusions and effusive/explosive eruptions (part 2: Observations). *Icarus*, *283*, 176–223. https://doi.org/10.1016/j.icarus.2016.05.031

Hiesinger, H., Head, J. W., Wolf, U., Jaumann, R., & Neukum, G. (2011). Ages and stratigraphy of lunar mare basalts: A synthesis. In W. A. Ambrose, & D. A. Williams (Eds.), *Recent advances and current research issues in lunar stratigraphy*, *Geological Society of America Special Paper 477* (pp. 1–51). Boulder, CO: Geological Society of America.

Kring, D. A. (2014). *Production of volatiles at lunar pyroclastic volcanic vents* (LPI Contribution No. 1820, abstract 3056). Laurel, MD: Paper presented at Annual Meeting of the Lunar Science Exploration Group.

Livengood, T. A., Mitrofanov, I. G., Chin, G., Boynton, W. V., Bodnarik, J. G., Evans, L. G., et al. (2018). Background and lunar neutron populations detected by LEND and average concentration of near-surface hydrogen near the Moon's poles. *Planetary and Space Science*, *162*, 89–104. https://doi.org/10.1016/j.pss.2017.12.004

Needham, D. H., & Kring, D. A. (2017). Lunar volcanism produced a transient atmosphere around the ancient moon. *Earth and Planetary Science Letters*, *478*, 175–178. https://doi.org/10.1016/j.epsl.2017.09.002

Newcombe, M. E., Brett, A., Beckett, J. R., Baker, M. B., Newman, S., Guan, Y., et al. (2017). Solubility of water in lunar basalt at low pH_2O. *Geochimica et Cosmochimica Acta*, *200*, 330–352. https://doi.org/10.1016/j.gca.2016.12.026

Ni, P., Zhang, Y., Chen, S., & Gagnon, J. (2019). A melt inclusion study on volatile abundances in the lunar mantle. *Geochimica et Cosmochimica Acta*, *249*, 17–41. https://doi.org/10.1016/j.gca.2018.12.034

Parfitt, E. A., & Wilson, L. (1995). Explosive volcanic eruptions-IX. The transition between hawaiian-style lava fountaining and strombolian explosive activity. *Geophysical Journal International*, *121*(1), 226–232. https://doi.org/10.1111/j.1365-246X.1995.tb03523.x

Pasckert, J. H., Hiesinger, H., & van der Bogert, C. H. (2015). Small-scale lunar farside volcanism. *Icarus*, *257*, 336–354. https://doi.org/10.1016/j.icarus.2015.04.040

Renggli, C. J., King, P. L., Henley, R. W., & Norman, M. D. (2017). Volcanic gas composition, metal dispersion and deposition during explosive volcanic eruptions on the moon. *Geochimica et Cosmochimica Acta*, *206*, 296–311. https://doi.org/10.1016/j.gca.2017.03.012

Rutherford, M. J., Head, J. W. III, Saal, A. E., Hauri, E. H., & Wilson, L. (2017). Model for the origin, ascent and eruption of lunar picritic magmas. *American Mineralogist*, *102*(10), 2045–2053. https://doi.org/10.2138/am-2017-5994

Rutherford, M. J., & Papale, P. (2009). Origin of basalt fire-fountain eruptions on earth versus the moon. *Geology*, *37*(3), 219–222. https://doi.org/10.1130/G25402a.1

Saal, A. E., Chaussidon, M., Gurenko, A. A., & Rutherford, M. J. (2018). *Boron and lithium contents and isotopic composition of the lunar volcanic glasses* (Vol. 49, abstract 2575). The Woodlands, TX: Paper presented at Lunar and Planetary Science Conference.

Saal, A. E., Hauri, E. H., Lo Cascio, M., Van Orman, J. A., Rutherford, M. C., & Cooper, R. F. (2008). Volatile content of lunar volcanic glasses and the presence of water in the Moon's interior. *Nature*, *454*(7201), 192–195. https://doi.org/10.1038/nature07047

Schulze-Makuch, D., & Crawford, I. A. (2018). Was there an early habitability window for Earth's moon? *Astrobiology*, *18*(8), 985–988. https://doi.org/10.1089/ast.2018.1844

Shearer, C. K., Hess, P. C., Wieczorek, M. A., Pritchard, M. E., Parmentier, E. M., Borg, L. E., et al. (2006). Thermal and magmatic evolution of the moon. *Reviews in Mineralogy and Geochemistry*, *60*(1), 365–518. https://doi.org/10.2138/rmg.2006.60.4

Solomon, S. C., & Head, J. W. III (1980). Lunar mascon basins: Lava filling, tectonics and evolution of the lithosphere. *Reviews of Geophysics and Space Physics*, *18*(1), 107–141. https://doi.org/10.1029/RG018i001p00107

Stern, S. A. (1999). The lunar atmosphere: History, status, current problems, and context. *Reviews of Geophysics*, *37*(4), 453–491. https://doi.org/10.1029/1999rg900005

Vondrak, R. R. (1974). Creation of an artificial lunar atmosphere. *Nature*, *248*(5450), 657–659. https://doi.org/10.1038/248657a0

Wallace, P. J., Plank, T., Edmonds, M., & Hauri, E. H. (2015). Volatiles in magmas. In H. Sigurdsson (Ed.), *The Encyclopedia of Volcanoes* (pp. 163–183). London, UK: Elsevier, Inc.

Weider, S. Z., Crawford, I. A., & Joy, K. H. (2010). Individual lava flow thicknesses in Oceanus Procellarum and Mare Serenitatis determined from Clementine multispectral data. *Icarus*, *209*(2), 323–336. https://doi.org/10.1016/j.icarus.2010.05.010

Whitten, J. L., & Head, J. W. III (2015a). Lunar cryptomaria: Mineralogy and composition of ancient volcanic deposits. *Planetary and Space Science*, *106*, 67–81. https://doi.org/10.1016/j.pss.2014.11.027

Whitten, J. L., & Head, J. W. III (2015b). Lunar cryptomaria: Physical characteristics, distribution, and implications for ancient volcanism. *Icarus*, *247*, 150–171. https://doi.org/10.1016/j.icarus.2014.09.031

Wieczorek, M. A., Neumann, G. A., Nimmo, F., Kiefer, W. S., Taylor, G. J., Melosh, H. J., et al. (2013). The crust of the moon as seen by GRAIL. *Science*, *339*(6120), 671–675. https://doi.org/10.1126/science.1231530

Wilson, L., & Head, J. W. III (1981). Ascent and eruption of basaltic magma on the earth and moon. *Journal of Geophysical Research*, *86*(B4), 2971–3001. https://doi.org/10.1029/JB086iB04p02971

Wilson, L., & Head, J. W. III (2003). Deep generation of magmatic gas on the moon and implications for pyroclastic eruptions. *Geophysical Research Letters*, *30*(12), 1605. https://doi.org/10.1029/2002GL016082

Wilson, L., & Head, J. W. III (2017). Generation, ascent and eruption of magma on the moon: New insights into source depths, magma supply, intrusions and effusive/explosive eruptions (part 1: Theory). *Icarus*, *283*, 146–175. https://doi.org/10.1016/j.icarus.2015.12.039

Wilson, L., & Head, J. W. III (2018). Controls on lunar basaltic volcanic eruption structure and morphology: Gas release patterns in sequential eruption phases. *Geophysical Research Letters*, *45*, 5852–5859. https://doi.org/10.1029/2018GL078327

Wilson, L., Head, J. W. III, & Zhang, F. (2019). A theoretical model for the formation of ring moat dome structures: Products of second boiling in lunar basaltic lava flows. *Journal of Volcanology and Geothermal Research*, *374*, 160–180. https://doi.org/10.1016/j.jvolgeores.2019.02.018